Journal of Marine Science and Application (2024) 23: 833-843
https://doi.org/10.1007/s11804-024-00472-9

RESEARCH ARTICLE

Evaluation of Chamfered Tank with Porous Walls Against Sloshing

Sepehr Partovi Sahneh[1], Hassan Saghi[2], Reza Saghi[3] and Mohammad Javad Ketabdari[1]

Received: 10 October 2023 / Accepted: 01 February 2024

Abstract

The sloshing in a tank with a specific geometric shape containing fluid was modeled numerically to reduce its effects by applying a porous medium to the tank wall. The thickness and position of the porous layer and the geometric shape of the tank were investigated as the main parameters to select an optimal approach to reduce the effects of sloshing. Different fluid tank filling percentages $\left(H_w/H_{tot}\right)$ were evaluated. Results indicate that performance at H_w/H_{tot} = 0.33 and two tank modes with and without a porous environment layer have the greatest impact on reducing sloshing. A thickness of 30 cm and placement on the side walls are determined to be the ideal thickness and location of the porous layer. A porous layer with a thickness (t) relative to the tank length at the middle (L_m), t/L_m= 0.1 applied to the side walls of the tank effectively reduces the pressure by 65%. This study provided suggestions for the aspect ratio of a chamfered tank designed against sloshing.

Keywords Sloshing; Chamfered tank; Porous layer; Baffle; VOF method; Numerical modeling

1 Introduction

Sloshing impacts the stability of various structures, such as fluid-carrying ships, and researchers have always been interested in modeling and providing solutions to control and reduce its effects. Modeling can be categorized as numerical or laboratory. Researchers have paid less attention to field research due to its high cost and risks. Instead, they have been using numerical methods to simulate this phenomenon. Numerical modeling requires selecting the governing equations, which involves determining whether the fluid's viscosity can be ignored or whether the fluid must be considered viscous. For some fluids, such as oil and gasoline, ideality is not possible. With water, viscosity is irrelevant, and this fluid can be considered ideal. Numerous researchers have assumed the fluid to be ideal for modeling sloshing (Choun and Yun, 1996; Fransden, 2004; Wu, 2007; Ketabdari and Saghi, 2013a; Saghi and Ketabdari, 2012; Saghi, 2016; Saghi et al., 2021). For instance, Ketabdari and Saghi (2013a) assumed the fluid was ideal and, therefore, used Laplace and Euler's equations. By employing boundary and finite elements and considering the noninfiltration of the tank body and the boundary conditions of the free surface of water, they were able to model sloshing in a rectangular and trapezoidal tank. This method solves the governing equations only on the tank wall's surface, and the parameter values within the fluid range can be determined using the boundary values. Many researchers have also assumed the fluid to be viscous and used Navier–Stokes equations to model the sloshing phenomenon (Saghi et al., 2020a; Saghi et al., 2020b, 2022; Saghi and Lakzian, 2017). For instance, Saghi and Mikkola (2020) assumed the fluid to be viscous and applied Navier–Stokes equations as the governing equations. The free surface was also modeled using the volume fraction method. Their study found that a diagonal dual baffle reduces sloshing impact by approximately 15% relative to that in the tank without a baffle.

To model sloshing, researchers proposed different geometric shapes for the storage tanks, including rectangular (Huang et al., 2010; Pirker et al., 2012), elliptical (Gavrilyuk et al., 2005), cylindrical (Papaspyrou et al., 2004; Shekari et al., 2009), circular conical (Gavrilyuk et al., 2005),

Article Highlights

- A numerical model was developed in the OpenFOAM software to simulate the sloshing phenomenon in a chamfered tank.
- The impact of employing a porous layer on the walls of a chamfered tank was assessed under various conditions.
- A chamfered tank with varying modeling dimensions and an optimal geometric shape was proposed based on the sloshing phenomenon.

✉ Hassan Saghi
hasansaghi1975@gmail.com

[1] Department of Marine Engineering, Amirkabir University of Technology, Tehran 15875-4413, Iran

[2] Department of Civil Engineering, Hakim Sabzevari University, Sabzevar 96179-76487, Iran

[3] State Key Laboratory of Coastal and Offshore Engineering, Dalian University of Technology, Dalian 116024, China

spherical (Yue 2008; Curadelli et al., 2010), and chamfer (Saghi et al., 2020b). Typical modeling methodologies have been used to simulate fluid flow parameters, such as velocity, pressure gradient, and free-surface displacement. As an example, Eswaran et al.(2011) experimentally investigated the unsteady free-surface velocities during the surge motion of a liquid tank. Papaspyrou et al. (2003) developed a mathematical model for calculating liquid sloshing effects, such as the hydrodynamic pressures and forces in half-full spherical containers under arbitrary external excitations. Sarreshtehdari et al. (2011) numerically and experimentally investigated the free-surface sloshing of liquid in a rectangular tank induced by lateral excitation. Mirzabozorg et al. (2012) examined the effect of free-surface sloshing on the dynamic response of rectangular storage tanks. In a partially filled automotive fuel tank, Rajagounder et al. (2016) studied the behavior of free-surface displacement under uniformly accelerated motion. Researchers have developed fluid methods to model the free surface. By using a new advection method, Saghi and Ketabdari(2014) presented a modified volume of the fluid method based on flux-correct transport and Young's method. For calculating curvature on free-surface flows, Saghi et al. (2013) presented a new method based on parameterization and used the volume of fluid method to capture surfaces for free-surface modeling.

Bubbles or cavities are generated during sloshing. Zhang et al. (2023) developed a theoretical framework for oscillating bubble dynamics, such as those occurring in cavitation bubbles, underwater explosion bubbles, and air bubbles. Thaker et al. (2020) studied sloshing on a shallow vessel and determined the effects of combined top and bottom gas injections and sloshing interfaces on gas-liquid flow dynamics and their role in liquid-phase mixing. A chamfered tank with porous walls is seriously impacted by cavities or bubbles, especially when it contains compressible fluids such as liquid natural gas. In modeling water in this research, we did not consider the effects of cavities and bubbles.

Sloshing is a destructive phenomenon that can negatively impact the performance of a wide range of structures. Therefore, its effects must be controlled and reduced. Many researchers have used various tools, such as a porous baffle and porous layer, which is placed on the tank surface to absorb the energy produced by sloshing. Xue et al. (2021) investigated the effect of a porous layer placed on the surface of a cylindrical tank on sloshing. Tsao and Huang (2021) analytically and experimentally investigated the effect of porous media on sloshing in a rectangular tank and showed that porous media can be used to control sloshing, especially in intensified circumstances. One of the new ways to control sloshing is to use foam. Zhang et al. (2019) investigated the antisloshing effects of floating solid foams in a rectangular tank and found that even a single layer of floating foams can reduce the first natural frequency of the fluid, thus reducing the sloshing range by energy loss caused by the interaction of neighboring foams. They also showed that using multiple layers of floating foams reduces the range of sloshing as the energy loss increases.

Recent studies have focused on the effects of the porous layer on sloshing in a tank. Xue et al. (2023) investigated the influences of porous baffles on reducing liquid sloshing in a rectangular tank. Dou et al. (2023) employed layers of porous media to enhance damping and suppress violent sloshing, and demonstrated that porous layers could dissipate the kinetic energy of fluids and suppress violent sloshing. According to the literature review, researchers have been less concerned with the effect of the porous layer's position within the reservoir. Therefore, the current research aims to reduce the effects of sloshing by examining the effects of using porous media in different parts of the chamfered tank and the optimal geometric section for this type of tank. Geometrical optimization is also conducted to determine the ideal geometry of the chamfered tank against sloshing.

2 Theory

This study modeled sloshing in a chamfered tank filled with an incompressible viscous fluid so that turbulent flow was considered. Reynolds averaged navier stokes equation (RANSE) was used as the governing equation (Dean and Dalrymple, 1991, and Saghi, 2018):

$$\nabla \cdot \left(\rho \underline{V}\right) = 0 \tag{1}$$

$$\frac{\partial}{\partial t}\left[\rho \underline{V}\right] + \nabla \cdot \left[\rho \underline{VV}\right] = -\nabla \underline{p} + \nabla \cdot \left[\underline{\tau} - \rho \underline{V'V'}\right] + \underline{f_b} \tag{2}$$

where ρ represents the fluid density; $\underline{V}$ is ensemble mean of velocity; ∇ is the gradient operator; $\underline{f_b}$ is body force; $\underline{p}$ is the dynamic pressure; τ is shear stress.

Pressure Implicit Method with Pressure Linked Equations (PIMPLE) is an algorithm developed for solving RANS equations. Various terms in the discretized equations, including derivatives, gradient parameters, Laplace derivatives, and divergence terms, were discretized with implicit Euler, centered Gauss linear, skewness corrected centered Gauss linear correction, and Upwind schemes, respectively (OpenFoam, 2019). Cartesian structured grid was generated in the domain using block mesh and refinement techniques to model a chamfered tank. Walls bound the study domain. Therefore, the movingWallVelocity Dirichlet boundary condition was used for the velocity field. For the pressure field and free-surface zone, fixedFluxPressure and zeroGradient Neumann boundary conditions were applied

(OpenFoam, 2019). In addition, the *K*-ε two-equation model was utilized to account for turbulence (Dean and Dalrymple, 1991).

$$\frac{\partial}{\partial t}\left[\rho k\right]+\frac{\partial}{\partial x_i}\left[\rho k u_i\right]=\frac{\partial}{\partial x_j}\left[\frac{\mu_t}{\sigma_k}\frac{\partial k}{\partial x_j}\right]+2\mu_t E_{ij}E_{ij}-\rho\varepsilon \quad (3)$$

$$\frac{\partial}{\partial t}\left[\rho\varepsilon\right]+\frac{\partial}{\partial x_i}\left[\rho\varepsilon u_i\right]=\frac{\partial}{\partial x_j}\left[\frac{\mu_t}{\sigma_\varepsilon}\frac{\partial\varepsilon}{\partial x_j}\right]+C_{1\varepsilon}\frac{\varepsilon}{k}2\mu_t E_{ij}E_{ij}-C_{2\varepsilon}\rho\frac{\varepsilon^2}{k} \quad (4)$$

where ε is dissipation rate; k is kinetic energy; E_{ij} is component of the deformation rate; x_i and x_j are the axis i and j directions, respectively; u_i is velocity components in i direction (x, y and z); t is time; and μ_t represents eddy viscosity, $\mu_t=\rho C_\mu\frac{k^2}{\varepsilon}$. The value of parameters $C_\mu=0.09$, $\sigma_k=1.0$, $C_{1\varepsilon}=1.44$, and $C_{2\varepsilon}=1.92$.

In the developed model, RANSE was discretized using the finite volume method, and equations were solved using the PIMPLE algorithm coupled with the volume of fluid (VOF). In the VOF method, parameter α, defined as Equation (5), was updated at each time step using Equation (6). This equation was solved via the multidimensional universal limiter for the explicit solution method (Rudman, 1997):

$$\begin{cases}\alpha=0, & \text{air}\\ \alpha=1, & \text{water}\\ 0<\alpha<1, & \text{inter facecell}\end{cases} \quad (5)$$

$$\frac{\partial\alpha}{\partial t}+\nabla\cdot\left[V\alpha\right]=0 \quad (6)$$

where α represents the volume fraction parameterr; and V is velocity vector;

A Multidimensional Universal Limited Explicit Solver was used to solve the VOF equation to describe phase movements (Ketabdari and Saghi, 2013b). The theoretical foundation for modeling fluid flow through porous media in OpenFOAM relies on Darcy's law, a fundamental principle governing fluid flow through porous materials using the following equation:

$$q=-\mu k_{\mathrm{d}}\left(\nabla P-C_f\cdot\rho V\right) \quad (7)$$

where C_{f} represents Forchheimer inertial resistance coefficient; P is pressure; μ is dynamic ciscosity; q is instantaneous flow rate; k_{d} is darcy permeability. k_{d} and C_{f} are material-dependent and must be determined through experimental testing or obtained from the literature for a given porous medium. For porous media, the simulation involves defining permeability (k_{d}) and the Forchheimer coefficient (C_{f}) to accurately represent porous medium. The topoSet utility was employed to identify and define where the porous medium model is applied.

3 Model calibration

3.1 Sloshing model validation

The validation of the numerical model begins with selecting the appropriate network dimensions and time step for solving the governing equations, which is called independence from the network and time step. Therefore, these two important things will be discussed first. A rectangular tank with a length of 0.874 m, a height of 0.535 m, and a thickness of 0.07 m was used, and sloshing was induced by a side movement with an amplitude of 0.075 m for 1.35 s. In this modeling, the water depth was assumed to be 0.2 m. The average dynamic pressure in the corner of the tank was used to compare the results related to different dimensions of the network. Figure 1 shows the results obtained for different numbers of grids. The use of cells with dimensions of 0.01 m (33 000 cells) was found to be acceptable.

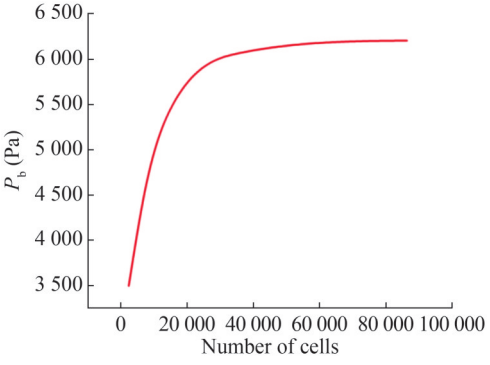

Figure 1 Average value of the dynamic pressure in the corner of the tank for different numbers of cells

In addition to the Courant number, the time step was automatically controlled by the model. At this stage, the developed model was used to simulate sloshing, and the results were evaluated against those presented by Kim et al. (2018) in Figure 2. The findings demonstrated the accuracy of the model.

3.2 Porous medium validation

In this step, the developed model was validated by modeling a tank with a porous boundary and under roll motion. The results presented by George and Cho (2021) were adopted. A rectangular tank with dimensions of 50 cm× 50 cm×10 cm was subjected to a roll movement with an amplitude of 0.5° and different periods, and the water depth

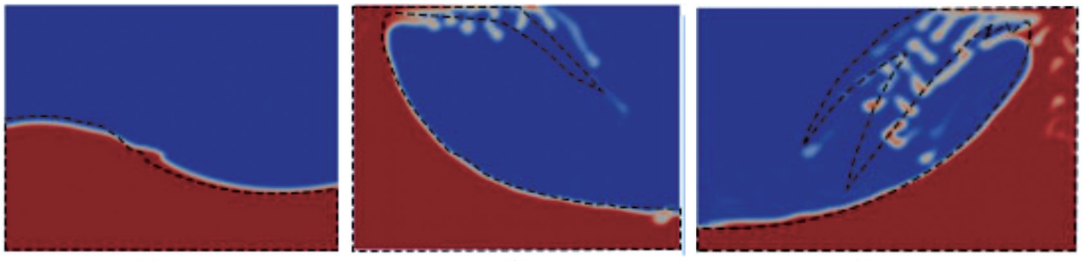

(a) 0.9 s (b) 2.0 s (c) 2.7 s

Figure 2 Comparison of the free surface caused by sloshing in a rectangular tank with a length of 0.874 m, a height of 0.535 m, and a width of 0.07 m containing water with a depth of 0.2 m due to side movement with an amplitude of 0.075 m and a period of 1.35 s at different times (Free surface of the background fluid: Present work; Dashed free surface: Kim et al. (2018))

was also 10 cm. The porous plate made of holes with radii of 1.5 and 8 mm (0.127 5% of porosity) was installed at a depth of 2 cm (Figure 3).

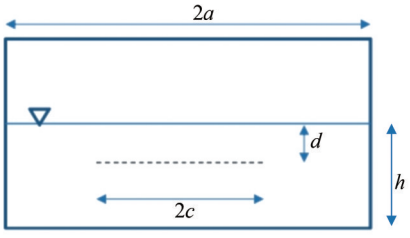

Figure 3 Storage tank modeled by George and Cho (2021) to evaluate the porous baffle against the sloshing impact.

In this stage, the difference between the maximum and minimum dynamic pressures at point $x = -a$ and $z = -0.8h$ was calculated, and the results are presented in Table 1. Here T is the roll movement period. The parameters a and h are shown in Figure 3. The model had an error of 3%–5%, which is acceptable.

For the second test scenario, the porous medium model was validated using the porous dam breaking test carried out by Liu et al. (1999). In Figure 4, the computational domain has the dimensions of 0.892 m by 0.58 m. A yellow-marked porous dam (0.29 m×0.37 m) was located at the center of the domain, and a reservoir with dimensions of 0.28 m× 0.25 m was situated at a 0.02 m distance. Furthermore, a red-marked initial water level of 0.025 m was established at the computational domain's base. Sen et al. (2022) stated that the coefficients of α, β, and c were 1 000, 1.1, and 0.34, respectively. Porous media n and D50 had the critical material characteristics of 0.49 and 0.015 9 m, respectively. The outcomes shown in Figure 4 show the reliability of the numerical approach. Figure 5 presents a comparison of fluid-front propagation between numerical and experimental results, showing good agreement between the two sets of data.

Table 1 Validation of the model based on the results presented by George and Cho (2021)

Method	$T = 0.45$ s	$T = 0.49$ s	$T = 0.59$ s	$T = 0.69$ s
George and Cho (2021)	440	450	325	250
Present work	425	466	314	263

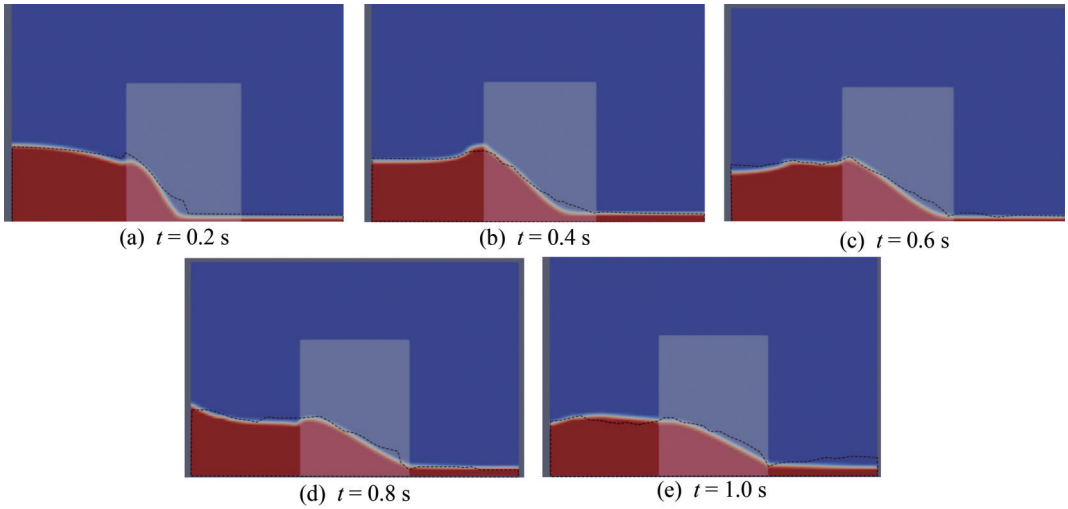

(a) $t = 0.2$ s (b) $t = 0.4$ s (c) $t = 0.6$ s

(d) $t = 0.8$ s (e) $t = 1.0$ s

Figure 4 Free-surface elevations for dam breaking processes using the developed model at different times (Free surface of the background fluid: Present work; Dashed free surface: Liu et al. (1999))

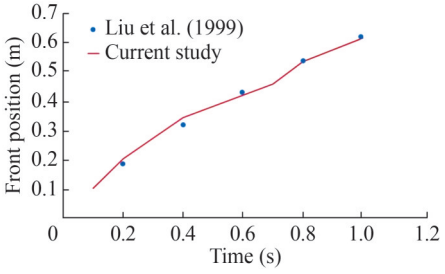

Figure 5 Comparison of fluid-front propagation between numerical and experimental results

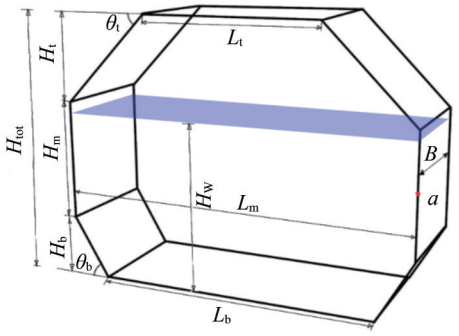

Figure 6 Schematic sketch of a chamfered tank (units: m)

4 Results

In this research, sloshing in a chamfered tank (Figure 6) is modeled and the results are discussed. First, we examine the porous layer on the left and right walls of the tank and its effect on sloshing.

4.1 Effect of porous layer thickness

First, a porous layer with a thickness of D is installed on the left and right walls of the tank, and a movement with an amplitude of 0.1 radians and a period of 0.5 s is then applied to the tank. Modeling is performed for 40 s. For the comparison of the results, the dynamic pressure on the right wall of the tank and the maximum horizontal force on the tank are used (See Figure 7). Then, the dynamic pressure value at point a (as shown in Figure 8(a)) and the horizontal force on the tank (Figure 8(b)) are used as the basis for comparing different scenarios. The dimensions of the tank shown in Figure 6 are $L_b = 2.4$ m, $L_m = 3$ m, $H_b = 0.5$ m, $L_t = 1.5$ m, $H_m = 1$ m, and $H_t = 0.75$ m, and the water depth is 0.75 m.

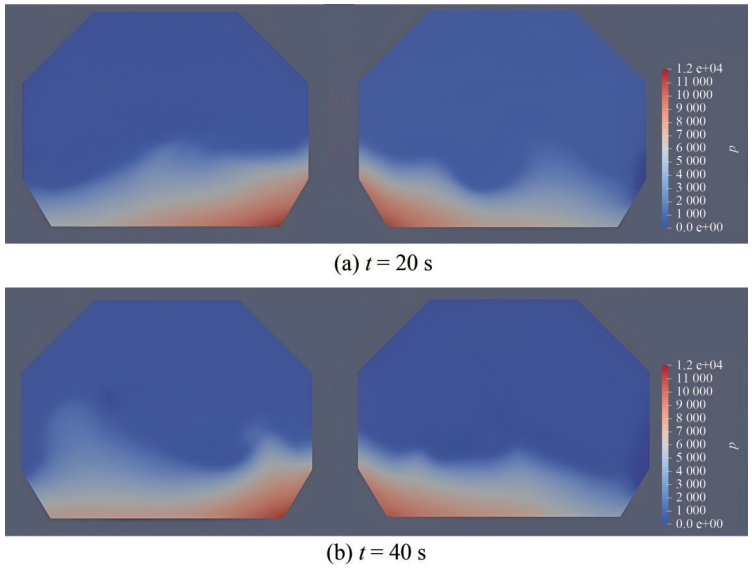

(a) $t = 20$ s

(b) $t = 40$ s

Figure 7 Dynamic pressure distribution inside the tank caused by sloshing at different times, and different thicknesses of the porous layer, left: $D = 0.1$ m, right: $D = 0.4$ m

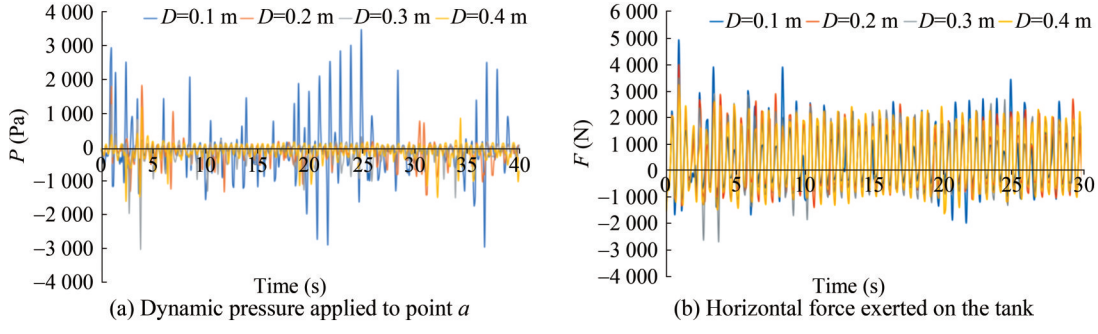

(a) Dynamic pressure applied to point a

(b) Horizontal force exerted on the tank

Figure 8 Comparison of the results obtained for different thicknesses of the porous layer

According to the obtained results, the maximum pressure and force exerted on the tank perimeter were calculated and shown in Figure 9.

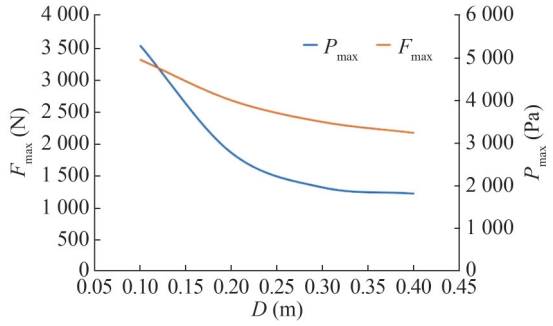

Figure 9 Comparison of the maximum pressure and horizontal force exerted on the tank perimeter for different porous thicknesses

The results shown in Figure 9 indicate that the thickness of the porous layer has a much greater effect on reducing the dynamic pressure than it does on reducing the horizontal force on the body. However, in the case of the model examined in this study, it was found that a thickness of 0.3 m is an acceptable thickness and that increasing the thickness beyond this value has little effect on reducing sloshing. Therefore, in the continuation of the research, the thickness of the porous layer is 0.3 m. To investigate the effects of the thickness of the porous layer on the velocity field, the flow velocity fields at 20 s in two cases of using a porous layer with a thickness of 0.1 m and 0.4 m are shown in Figure 10. The obtained results indicate the significant effects of using porous layer on speed reduction.

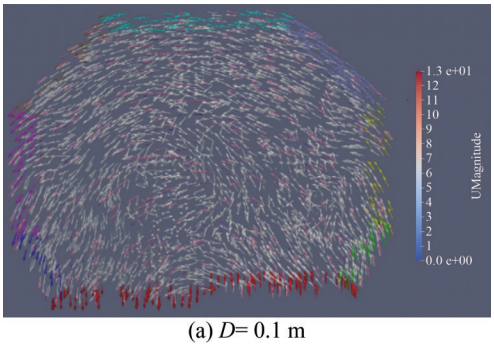

(a) D= 0.1 m

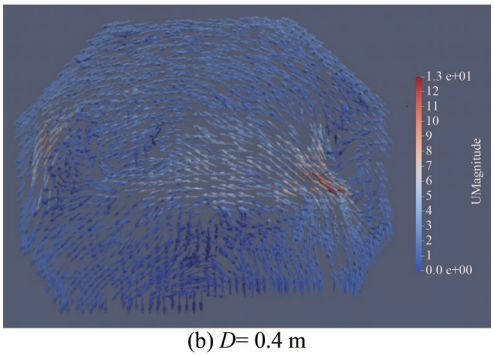

(b) D= 0.4 m

Figure 10 Comparison of the velocity field for different values of the thickness of the porous layer at t = 20 s

4.2 Effect of the position of the porous layer

The effect of the position of the porous medium layer on the performance of the tank under sloshing conditions is examined. Figure 11 illustrates different placements of the porous layer, including on the bottom of the tank, the roof of the side walls, and the entire surface of the tank. The performance of the tank is compared with that of the tank without the porous layer. Figure 12 shows the distribution of dynamic pressure at different points of the fluid and for different scenarios over a time of 40 s.

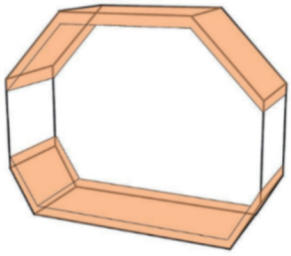

(a) Top and bottom

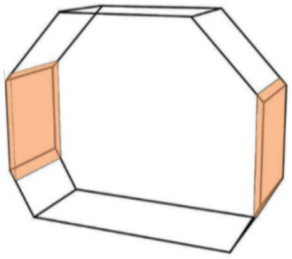

(b) Left and right

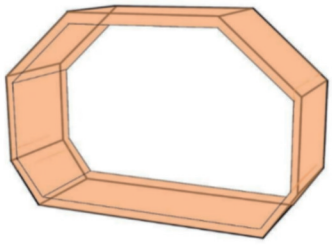

(c) All body

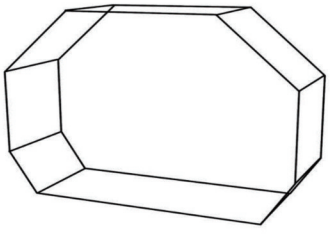

(d) Without porous layer

Figure 11 Different scenarios of porous layer placement

On the basis of the obtained results, the dynamic pressure at point a is calculated for different states and shown in Figure 13.

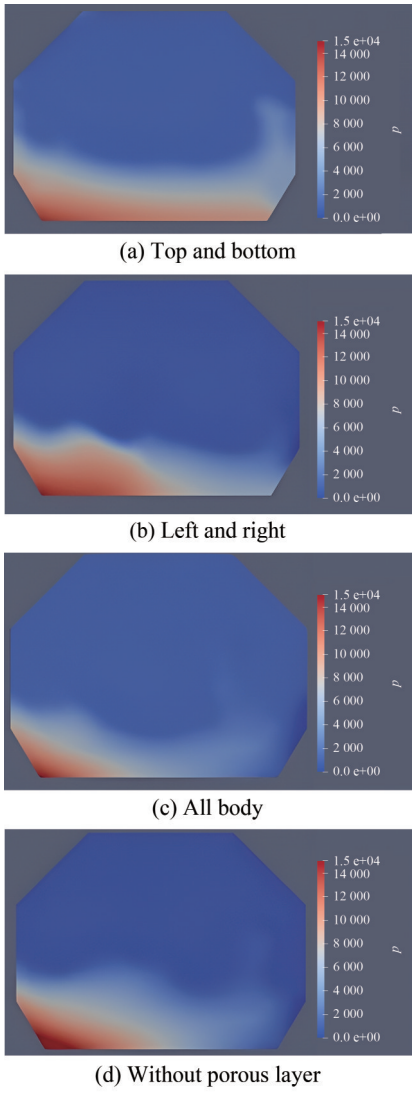

Figure 12 Pressure distribution in the tank for different scenarios of porous layer placement

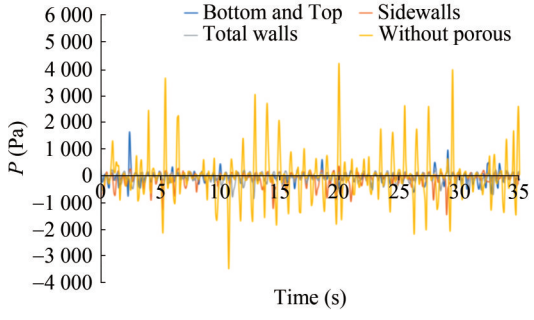

Figure 13 Time history of the pressure at point *a* in the tank for different scenarios of porous layer placement

Figure 12 shows that placing a porous medium on the floor and roof of the tank reduces the dynamic pressure by 60% compared with that in the tank without a porous layer. In addition, placing a porous layer on the side walls and on the entire wall of the tank reduces the dynamic pressure by 65% and 75%, respectively. In the next step, the effects of placing the porous layer on the entire wall of the tank are evaluated at different water depths. Changes in dynamic pressure at point *a* and at different times are calculated for different water depths and at different times. As an example, the results obtained at $t = 10$ s are presented in Figure 14. The calculated dynamic pressure at point *a* for different states is shown in Figure 15.

The maximum dynamic pressure applied to the tank at the desired point is calculated for the tanks with different filling percentages and with or without a porous layer, and the results are shown in Figure 16.

The results show that the porous layer has a strong dependence on the height of the water in the tank. The maximum effectiveness of the porous layer is observed at a depth of 0.75 m. In this situation, the existence of the porous layer can reduce the dynamic pressure by approximately 75%. Meanwhile, the amount of dynamic pressure reduction in the depth of 0.5 m is approximately 50%.

4.3 Geometrical analysis of the tank

In this section, we examine the effect of the geometric shape of the tank. Different scenarios are considered for tank dimensions so that all tanks have a constant volume. The performance of the tanks with and without a porous layer is investigated. In addition to choosing the optimal section, the effect of using a porous layer in different scenarios is also analyzed. Table 2 summarizes the geometric parameters of the chamfered tank used in the numerical simulation (Figure 6).

The amount of dynamic pressure at point *a* on the body of the tank in different states is checked by modeling all the tanks. As an example, the results for several cases and for the tanks with and without a porous layer on the walls are shown in Figures 17 and 18, respectively.

In this step, the maximum dynamic pressure is calculated and analyzed based on the obtained results and then used as a basis for comparing different scenarios. The obtained results are given in Figure 19.

The results show that scenario 15 has better performance than the other scenarios in two cases (with and without the porous layer on the wall). The greatest impact of the presence of the porous layer on the wall can be determined by comparing the results of two cases and the amount of dynamic pressure reduction in the tank with or without the porous layer on the wall. Scenario 15 still appears to be the best scenario. To provide design options, we determine the dimensionless parameters for tank design according to the geometric dimensions of the tank. Figure 20 shows the dimensionless geometric parameters of the tank for different scenarios.

As shown in Figure 20 and on the basis of the selected scenario (Scenario 15), the optimal dimension ratio for the tank is suggested as dimensionless parameters $H_b/H_t = 0.75$ and $L_b/L_t = 1.25$.

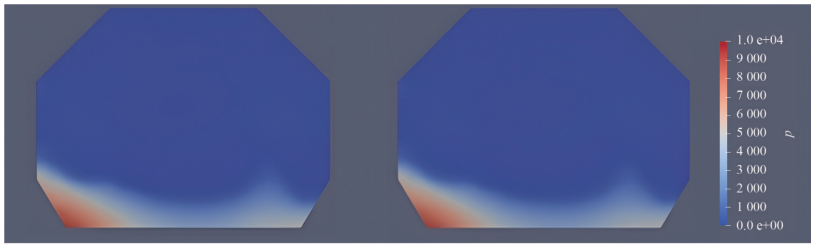

(a) H_w = 0.50 m

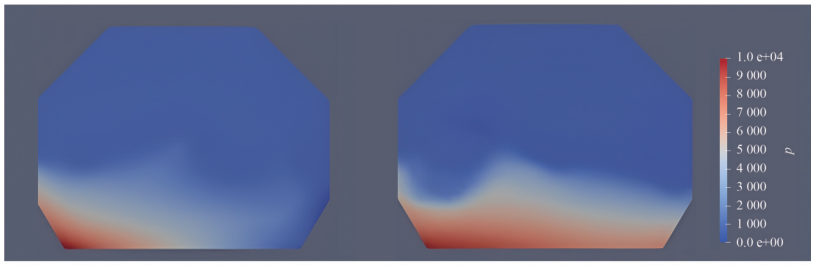

(b) H_w = 0.75 m

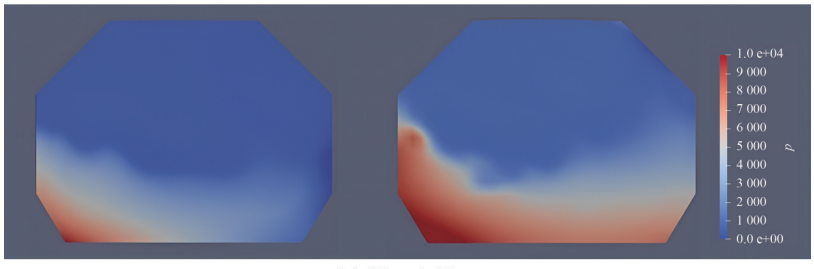

(c) H_w = 1.00 m

Figure 14 Dynamic pressure distribution in the tank at different water depths (H_w) in 10 s: with porous layer (left) and without porous layer (right)

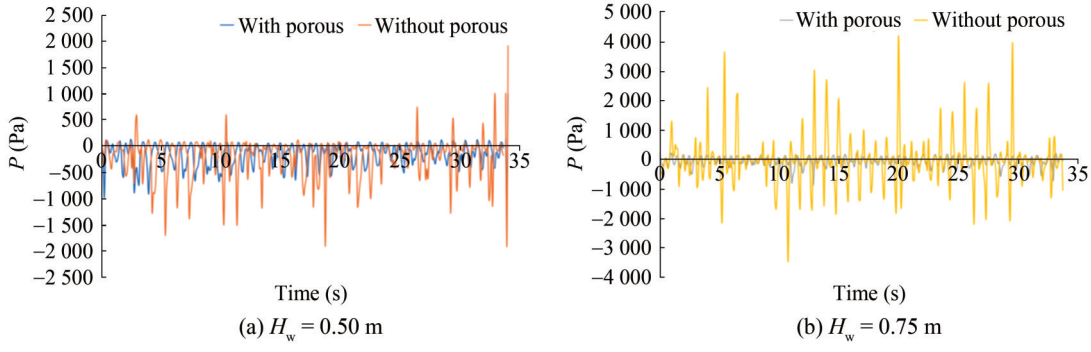

(a) H_w = 0.50 m (b) H_w = 0.75 m

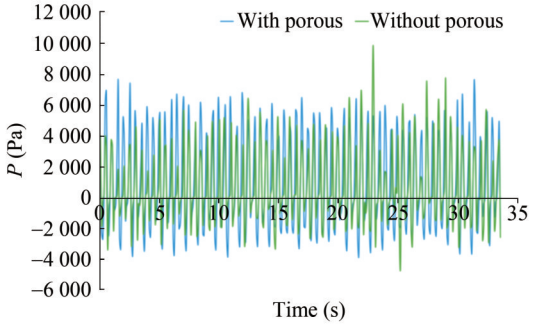

(c) H_w = 1.00 m

Figure 15 Comparison of the dynamic pressure distribution in the tank with and without porous layer and for different filling percentages

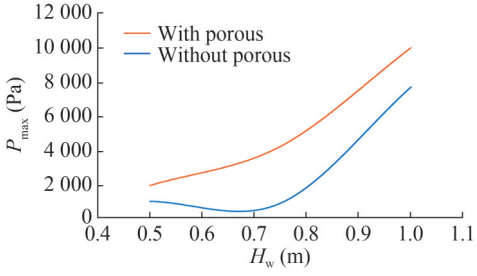

Figure 16 Maximum dynamic pressure at point *a* for different water depths and tanks with and without a porous layer

Table 2 Scenarios investigated by the geometric analysis of the tank

Scenario number	H_b (m)	H_m (m)	H_t (m)	L_b (m)	L_m (m)	L_t (m)	θ_b (°)	θ_t (°)
1	0.5	1.0	0.73	2.4	3.0	1.5	59	44
2	0.5	1.0	0.72	2.4	3.0	1.6	59	46
3	0.5	1.0	0.70	2.4	3.0	1.7	59	47
4	0.5	1.0	0.69	2.4	3.0	1.8	59	49
5	0.5	1.0	0.68	2.4	3.0	1.9	59	51
6	0.5	1.0	0.66	2.4	3.0	2.0	59	53
7	0.5	1.0	0.65	2.4	3.0	2.1	59	55
8	0.5	1.0	0.64	2.4	3.0	2.2	59	58
9	0.5	1.0	0.63	2.4	3.0	2.3	59	61
10	0.5	1.0	0.75	2.4	3.0	2.4	59	68
11	0.51	1.0	0.75	2.3	3.0	1.5	56	45
12	0.52	1.0	0.75	2.2	3.0	1.5	52	45
13	0.53	1.0	0.75	2.1	3.0	1.5	50	45
14	0.54	1.0	0.75	2.0	3.0	1.5	47	45
15	0.55	1.0	0/.75	1.9	3.0	1.5	45	45
16	0.56	1.0	0.75	1.8	3.0	1.5	43	45
17	0.57	1.0	0.75	1.7	3.0	1.5	41	45
18	0.59	1.0	0.75	1.6	3.0	1.5	40	45
19	0.60	1.0	0.75	1.5	3.0	1.5	39	45
20	0.61	1.0	0.75	1.4	3.0	1.5	37	45

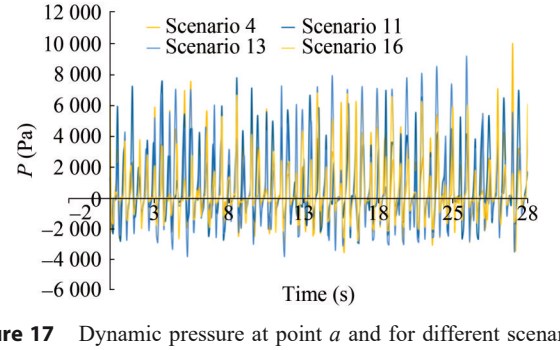

Figure 17 Dynamic pressure at point *a* and for different scenarios in the presence of the porous layer on the wall

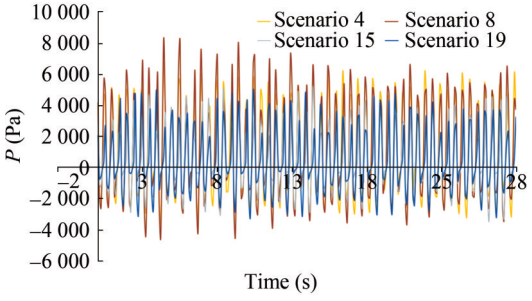

Figure 18 Dynamic pressure at point *a* and for different scenarios in the absence of the porous layer on the wall

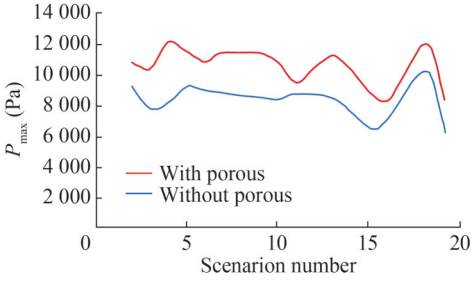

Figure 19 Maximum dynamic pressure on the tank body at point *a* for different scenarios and for the tank with and without a porous layer on the wall

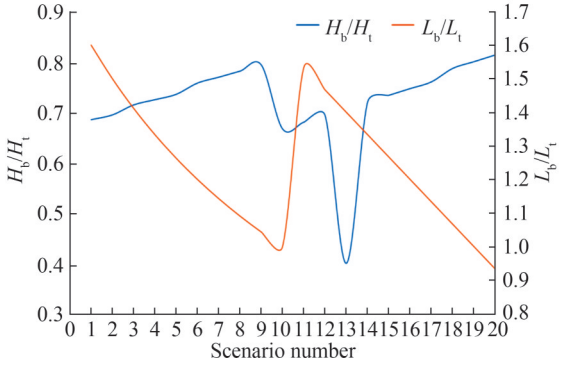

Figure 20 Dimensionless tank geometry parameters for different scenarios

5 Conclusions and discussion

The effects of sloshing on tanks with a chamfered section have been investigated by developing a numerical model that can simulate this phenomenon in the tank caused by the roll movement. The behavior of the tank in different conditions, including the roll movement with different domains, has also been studied. Dynamic pressure and force on the tank body have been used as the main criteria to compare different scenarios. A porous layer was placed on different parts of the tank walls. After the optimal thickness was chosen, the performance of the porous layer was investigated in different conditions. The results showed that increasing the thickness of the porous layer

on the wall (which was used only on the side walls in the first case) reduces the effects of sloshing. However, as the thickness increases from 30 cm, the effects of using the porous medium gradually decrease. Therefore, a relative thickness of the porous layer (D) to the tank length at the middle (L_m), $\frac{D}{L_m} = 0.1$ effectively reduces the pressure by 65%. In the continuation of the research, the effect of placing the porous layer in different parts of the tank was also investigated. A porous layer with a thickness of 30 cm was installed on the side walls, floor, and ceiling of the tank and in all the walls of the tank, and its effect on sloshing was investigated. The results showed that placing the porous layer on the tank floor and roof reduces the dynamic pressure by 60% compared with that in the tank without a porous layer. In addition, placing the porous layer on the side walls and on the entire wall of the tank reduces the dynamic pressure by 65% and 75%, respectively. Therefore, the effects of placing the porous layer in different parts of the tank can be observed.

Competing interest The authors have no competing interests to declare that are relevant to the content of this article.

References

Choun YS, Yun CB (1996). Sloshing characteristics in rectangular tanks with a submerged block. Computers & Structures 61: 401-413. https://doi.org/10.1016/0045-7949(96)00084-3

Curadelli O, Ambrosini D, Mirasso A, Amani M (2010) Resonant frequencies in an elevated spherical container partially filled with water: FEM and measurement. Journal of Fluids and Structures 26(1):148-159. https://doi.org/10.1016/j.jfluidstructs.2009.10.002

Dou PD, Xue NA, Zheng J, Chen M (2023) Study on suppression of violent sloshing in a multiple tuned liquid column damper by porous media layers. Ocean Engineering 289:116212

Dean RG, Dalrymple RA (1991) Water wave mechanics for engineers and scientists. Advanced Series on Ocean Engineering: Volume 2. https://doi.org/10.1142/1232

Eswaran M, Singh A, Saha UK (2011) Experimental measurement of the surface velocity field in an externally induced sloshing tank. Proceedings of the Institution of Mechanical Engineers, Part M: Journal of Engineering for the Maritime Environment 225(2): 133-148. https://doi.org/10.1177/1475090211402288

Fransden JB (2004) Sloshing motions in excited tanks. Journal of Computational Physics 196(1): 53-87. https://doi.org/10.1016/j.jcp.2003.10.031

Gavrilyuk IP, Lukovsky IA, Timokha AN (2005) Linear and nonlinear sloshing in a circular conical tank. Fluid Dynamics Research 37: 399-429. https://doi.org/10.1016/j.fluiddyn.2005. 08.004

George A, Cho IH (2021) Anti-slosh effect of a horizontal porous baffle in a swaying/rolling rectangular tank: Analytical and experimental approache. International Journal of Naval Architecture and Ocean Engineering 13: 833-847. https://doi.org/10.1016/j.ijnaoe.2021.10.001

Huang S, Duan WY, Zhu X (2010) Time-domain simulation of tank sloshing pressure and experimental validation. Journal of Hydrodynamics Ser. B. 22(5, Supplement 1) :556-563. https://doi.org/10.1016/S1001-6058(09)60252-3

Kim SP, Chung SM, Shin WJ, Chou DS, Park JC (2018) Experimental study on sloshing reduction effects of baffles linked to a spring system. Ocean Engineering 170: 136-147. https://doi.org/10.1016/j.oceaneng.2018.10.001

Ketabdari MJ, Saghi H (2013a) Parametric study for optimization of storage tanks considering sloshing phenomenon using coupled BEM – FEM. Applied Mathematics and Computation 224: 123-139. https://doi.org/10.1016/j.amc.2013.08.036

Ketabdari MJ, Saghi H (2013b) Development of volume of fluid methods to model free surface flow using new advection algorithms. J Braz Soc Mech Sci Eng. 35: 479-491. https://doi.org/10.1007/s40430-013-0045-7

Liu PLF, Lin PZ, Chang KA, Sakakiyama T (1999) Numerical modeling of wave interaction with porous structures. J. Waterway Port Coast. 125: 322-330. https://doi.org/10.1016/j.apor.2020.102522

Mirzabozorg H, Hariri Ardebili M, Nateghi R (2012) Free surface sloshing effect on dynamic response of rectangular storage tanks. American Journal of Fluid Dynamics 14 2(4): 23-30. https://doi.org/10.5923/j.ajfd.20120204.01

OpenFoam (2019) The openFoam Foundation, User Guide. http://openfoam.org

Papaspyrou S, Karamanos SA, Valougeorgis D (2004) Response of half-full horizontal cylinders under transverse excitation. Journal of Fluids and Structures 19(7): 985-1003. https://doi.org/10.1016/j.jfluidstructs.2004.04.014

Papaspyrou S, Valougeorgis D, Karamanos S (2003) Refined Solutions of Externally Induced Sloshing in Half-Full Spherical Containers. J. Eng. Mech. 129:1369-1379. https://doi.org/10.1061/(ASCE)0733-9399(2003)129:12(1369)

Pirker S, Aigner A, Wimmer G (2012) Experimental and numerical investigation of sloshing resonance phenomena in a spring-mounted rectangular tank. Chemical Engineering Science 68(1): 143-150. https://doi.org/10.1016/j.ces.2011.09.021

Rajagounder R, Vignesh Mohanasundaram G, Kalakkath P (2016) A Study of Liquid Sloshing in an Automotive Fuel Tank under Uniform Acceleration. Engineering Journal 20(1): 71-85. https://doi.org/10.4186/ej.2016.20.1.71

Rudman M (1997) Volume-tracking methods for interfacial flow calculation. Int. J. Numer. Methods Fluids 24:671-691.https://doi.org/10.1002/(SICI)1097-0363(19970415)24:7<671::AID-FLD508>3.0.CO;2-9

Saghi H, Ketabdari MJ (2012) Numerical simulation of sloshing in rectangular storage tank using coupled FEM-BEM. Journal of Marine Science and Application 11: 417-426. https://doi.org/10.1007/s11804-012-1151-0

Saghi H (2016) The pressure distribution on the rectangular and trapezoidal storage tanks' perimeters due to liquid sloshing phenomenon. International Journal of Naval Architecture and Ocean Engineering 8: 153-168 .https://doi.org/10.1016/j.ijnaoe.2015.12.001

Saghi R, Hirdaris S, Saghi H (2021) The influence of flexible fluid structure interactions on sway induced tank sloshing dynamics. Engineering Analysis with Boundary Elements 131: 206-217. https://doi.org/10.1016/j.enganabound.2021.06.023

Saghi H, Mikkola T, Hirdaris S (2020a) The influence of obliquely perforated dual baffles on sway induced tank sloshing dynamics, Proceedings of the Institution of Mechanical Engineers, Part M: Journal of Engineering for the Maritime Environment 235(4): 905-920. https://doi.org/10.1177/1475090220961920

Saghi H, Ning D, Pan S, Saghi R (2022) Optimization of a dual-baffled rectangular tank against the sloshing phenomenon. Journal of Marine Science and Application 21: 116-127. https://doi.org/10.1007/s11804-022-00257-y

Saghi H, Ning DZ, Cong PW, Zhao M (2020b) Optimization of Baffled Rectangular and Prismatic Storage Tank Against the Sloshing Phenomenon. China Ocean Engineering 34: 664-676. https://doi.org/10.1007/s13344-020-0059-8

Saghi H, Lakzian E (2017) Optimization of the rectangular storage tanks for the sloshing phenomena based on the entropy generation minimization. Energy 128l: 564-574. https://doi.org/10.1016/j.energy.2017.04.075

Saghi H (2018) Entropy generation minimization for the sloshing phenomenon in half-full elliptical storage tanks. Physica A: Statistical Mechanics and its Applications 491: 972-983. https://doi.org/10.1016/j.physa.2017.09.086

Shekari MR, Khaji N, Ahmadi MT (2009) A couple BE-FE study for evaluation of seismically isolated cylindrical liquid storage tanks considering fluid-structure interaction. Journal of Fluids and Structures 25(3): 567-585. https://doi.org/10.1016/j.jfluidstructs.2008.07.005

Sarreshtehdari A, Shahmardan MM, Gharaei R (2011) Numerical simulation and experimental validation of free surface sloshing in a rectangular tank. Journal of Solid and Fluid Mechanics 1(1): 89-95. https://doi.org/10.22044/JSFM.2012.30

Saghi H, Ketabdari MJ (2014) A modification to SLIC and PLIC volume of fluid models using new 19 advection method. Arab J. Sci. Eng. 39(2): 669-684. https://doi.org/10.1007/s13369-013-0688-9

Saghi H, Ketabdari MJ, Zamirian M (2013) A novel algorithm based on parameterization method 21 for calculation of curvature of the free surface flows. Applied Mathematical Modeling 37(1-2): 570-585. https://doi.org/10.1016/j.apm.2012.02.043

Sen W, Xu T, Dong G, Wang T, Chen L (2022) Numerical simulation of anti-sloshing performance in a 2D rectangular tank with random porous layer. Ocean Eng. 265: 112660. https://doi.org/10.1016/j.oceaneng.2022.112660

Tsao WH, Huang YL (2021) Sloshing force in a rectangular tank with porous media. Results in Engineering 11: 100250. https://doi.org/10.1016/j.rineng.2021.100250

Thaker AH, Bhujbal SV, Buwa VV (2020) Effects of sloshing gas–liquid interface on dynamics of meandering bubble plumes and mixing in a shallow vessel: PIV and PLIF measurements. Chemical Engineering Journal 386: 122036. https://doi.org/10.1016/j.cej.2019.122036

Wu GX (2007) Second-order resonance of sloshing in a tank. Ocean Engineering 34(17-18): 2345-2349. https://doi.org/10.1016/j.oceaneng.2007.05.004

Xue MA, Jiang Z, Lin P, Zheng J, Yuan X, Qian L (2021) Sloshing dynamics in cylindrical tank with porous layer under harmonic and seismic excitations. Ocean Engineering 235: 109373. https://doi.org/10.1016/j.oceaneng.2021.109373

Xue A, He Y, Yuan X, Cao Z, Odoom JK (2023) Numerical and experimental study on sloshing damping effects of the porous baffle. Ocean Engineering 285: 115363. https://doi.org/10.1016/j.oceaneng.2023.115363

Yue BZ (2008) Nonlinear coupling dynamics of liquid filled spherical container in microgravity. Applied Mathematics and Mechanics 29: 1085-1092. https://doi.org/10.1007/s10483-008-0812-y

Zhang C, Su P, Ning D (2019) Hydrodynamic study of an anti-sloshing technique using floating foams. Ocean Engineering 175: 62-70. https://doi.org/10.1016/j.oceaneng.2019.02.014

Zhang MA, Li SM, Cui P, Li S, Liu YL (2023) A unified theory for bubble dynamics. Physics of Fluids 35(3): 033323. https://doi.org/10.1063/5.0145415